

## Electrochemistry of Manganese Dioxide in Lithium Nonaqueous Cell: I . X-Ray Diffractational Study on the Reduction of Electrolytic Manganese Dioxide

To cite this article: Tsutomu Ohzuku *et al* 1989 *J. Electrochem. Soc.* **136** 3169

View the [article online](#) for updates and enhancements.

### You may also like

- [The Population of Oxygen Vacancies in  \$\text{Li}\_{1-x}\text{Mn}\_x\text{O}\_4\$  Type Cathode Materials: The Primary Factor of Temperature Dependent Structural Changes](#)  
X. Q. Yang, X. Sun, M. Balasubramanian et al.
- [A Reversible Lithium Intercalation Process in an  \$\text{ReO}\_3\$  Type Structure  \$\text{PNb}\_3\text{O}\_{25}\$](#)   
Sébastien Patoux, Mickael Dolle, Gwenaëlle Rousse et al.
- [Topotactic Two-Phase Reactions of  \$\text{Li}\[\text{Ni}\_{1/2}\text{Mn}\_{3/2}\text{O}\_4 \(P4\_32\)\]\$  in Nonaqueous Lithium Cells](#)  
Kingo Ariyoshi, Yasunobu Iwakoshi, Noriaki Nakayama et al.



### Your Lab in a Box!

The PAT-Tester-i-16: All you need for Battery Material Testing.

- ✓ All-in-One Solution with integrated Temperature Chamber!
- ✓ Cableless Connection for Battery Test Cells!
- ✓ Fully featured Multichannel Potentiostat / Galvanostat / EIS!

[www.el-cell.com](http://www.el-cell.com) +49 40 79012-734 [sales@el-cell.com](mailto:sales@el-cell.com)

  
electrochemical test equipment



$V = 3.7-2.2 = 1.5$  is substituted in Eq. [A-1], the Li insertion amount at the bending point is obtained

$$e_1 = Vx/m = 1.79x \quad (\text{calculated line 3 in Fig. 3})$$

#### REFERENCES

1. B. Scrosati, *Electrochim. Acta*, **26**, 1559 (1981).
2. K. M. Abraham, *J. Power Sources*, **7**, 1 (1981/1982).
3. A. J. Jacobson, R. R. Chianelli, and M. S. Whittingham, *This Journal*, **126**, 2277 (1979).
4. A. J. Jacobson, R. R. Chianelli, S. M. Rich, and M. S. Whittingham, *Mater. Res. Bull.*, **14**, 1437 (1979).
5. K. S. Liang, J. P. deNeufville, A. J. Jacobson, R. R. Chianelli, and F. Betts, *J. Non-Cryst. Solids*, **35**, and **36**, 1249 (1980).
6. A. J. Jacobson and S. M. Rich, *This Journal*, **127**, 779 (1980).
7. K. M. Abraham and S. B. Brummer, in "Lithium Batteries," J. P. Gabano, Editor, p. 371, Academic Press, London (1983).
8. J. J. Auborn, Y. L. Barberio, K. J. Hanson, D. M. Schleich, and M. J. Martin, *This Journal*, **134**, 580 (1987).
9. Y. Takeda, R. Kanno, Y. Tsuji, and O. Yamamoto, *ibid.*, **131**, 2006 (1984).
10. O. Bohnke and G. Robert, *Solid State Ionics*, **6**, 1155 (1982).
11. F. Bonino, L. P. Bicelli, R. Rivolta, M. Lazzari, and F. Festorazzi, *ibid.*, **17**, 21 (1985).
12. K. Nassau and D. W. Murphy, *J. Non-Cryst. Solids*, **44**, 297 (1981).
13. T. Pagnier, M. Fouletier, and J. L. Souguet, *Mater. Res. Bull.*, **18**, 609 (1983).
14. T. Pagnier, M. Fouletier, and J. L. Souguet, *Solid State Ionics*, **9** and **10**, 649 (1983).
15. Y. Sakurai and J. Yamaki, *This Journal*, **132**, 512 (1985).
16. Y. Sakurai and J. Yamaki, *ibid.*, **135**, 791 (1988).
17. S. Yamagata, T. Miura, T. Kishi, and T. Nagai, in "Proceedings of Electrochemical Society of Japan," F107 (1983).
18. M. Levy, M. J. Duclot, and F. Rousseau, in "Extended Abstracts of the International Meeting on Lithium Batteries," PA-18 (1988).
19. Y. Sakurai, S. Okada, J. Yamaki, and T. Okada, *J. Power Sources*, **20**, 173 (1987).
20. S. Okada and J. Yamaki, *This Journal*, In press.

## Electrochemistry of Manganese Dioxide in Lithium Nonaqueous Cell

### I. X-Ray Diffractational Study on the Reduction of Electrolytic Manganese Dioxide

Tsutomu Ohzuku,\* Masaki Kitagawa, and Taketsugu Hirai\*

*Electrochemistry and Inorganic Chemistry Laboratory, Department of Applied Chemistry, Faculty of Engineering, Osaka City University, Sumiyoshi, Osaka 558, Japan*

#### ABSTRACT

X-ray diffractational (XRD) studies were carried out for the electrochemical reduction of heat-treated electrolytic  $\text{MnO}_2$  (250° and 400°C for 7 days). A series of XRD examinations indicated that the reaction proceeded without the destruction of the core structure of electrolytic manganese dioxide (EMD). The structural changes during the electrochemical reductions of both EMDs were described, assuming a tetragonal sublattice. Both heat-treated electrolytic  $\text{MnO}_2$ s (HEMDs) behaved similarly in the tetragonal sublattice parameter *vs.* the reduction degree plots. During the first half of the reduction, HEMD phase having a tetragonal sublattice ( $a = 4.39-4.40\text{Å}$ ,  $c = 2.86-2.90\text{Å}$ ) was converted into a new  $\text{Li}_x\text{MnO}_2$  phase having an expanded tetragonal sublattice ( $a = 4.9-5.0\text{Å}$ ,  $c = 2.82-2.86\text{Å}$ ), *i.e.*, in a two-phase reaction. In the 30-90% reduction, the *a*-axis increased continuously as a function of reduction degree, *i.e.*, in a homogeneous phase reaction. The possible crystal structure of the deep discharge product  $\text{Li}_x\text{MnO}_2$  ( $x > 0.8$ ) is discussed, assuming a tetragonal unit cell ( $a = \text{ca. } 5\text{Å}$ ,  $c = \text{ca. } 2.85\text{Å}$ ) having the NiAs-type structure by analogy with  $\text{Li}_x\text{RuO}_2$ , and an orthorhombic unit cell, *i.e.*,  $a = 2 \times b\text{Å}$ ,  $b = \text{ca. } 5\text{Å}$ ,  $c = \text{ca. } 2.85\text{Å}$ . From these, assuming an orthorhombic unit cell having  $a = 10.27\text{Å}$ ,  $b = 4.93\text{Å}$ , and  $c = 2.85\text{Å}$ , all diffraction lines from the reduction products of HEMD were indexed.

Electrolytic manganese dioxide (EMD) is one of the most important materials for both aqueous and nonaqueous cells. Extensive research has been done to understand the electrochemistry of EMD in aqueous solution. Few papers, however, have dealt with the electrochemistry of EMD in lithium nonaqueous cells, partly because the lithium/manganese dioxide cell is a newly developed system compared with conventional aqueous cell systems, but mainly because the specific crystal structure of EMD, which is essential to understanding the electrochemistry of EMD, is not known. Since EMD contains large amounts of water, EMD cannot be used in lithium nonaqueous cells unless undesirable water is removed. In order to remove such undesirable water, and hopefully to give an appropriate structure of EMD for lithium nonaqueous cell applications, Ikeda *et al.* (1-4) proved the value of the heat-treatment of EMD and commercially established the lithium/manganese dioxide primary cell. The effect of heat-treatment, however, upon the cell performance, combined with the structural changes as a function of temperature, has been still a source of dispute among several authors (5-9).

Reaction mechanisms of heat-treated EMDs (HEMDs) have been examined by using electrochemical and analyti-

cal techniques and have been proposed in different ways (5, 6, 10). However, little is known about the reduction mechanism of HEMD, especially in relation to the crystal structure of EMD. In this paper, we report results on the electrochemical discharge, open-circuit voltage, and detailed x-ray diffractational measurements, and discuss the reduction mechanism of HEMD in lithium nonaqueous cells, assuming a tetragonal sublattice to represent EMD structure and its reduced form.

#### Experimental

**Samples.**—An EMD, having a particle size of 60-100 mesh and an equi-acidic point of 2.23 on the pH scale, was obtained from TOSOH and well washed with distilled water at 85°-95°C for a week in a Soxhlet extractor. The washed EMD was dried at  $80^\circ \pm 3^\circ\text{C}$  for 2 days, and ground to a particle size below 200 mesh. The heat-treated EMDs (HEMDs) were prepared by heat-treatment of pre-dried EMD in air at 250°C [HEMD(250)] or 400°C [HEMD(400)] for 7 days. Thus obtained HEMD samples were characterized by x-ray diffraction (XRD) (Type XD-3A, Shimadzu Corporation Japan) and chemical analysis.

**Electrochemical cell.**—A flooded experimental cell consisted of a lithium anode ( $15 \times 20\text{ mm}^2$ ) and a HEMD cathode ( $15 \times 20\text{ mm}^2$ ) separated by a polypropylene non-

\*Electrochemical Society Active Member.

woven cloth (FT-330, Byrean, Japan). The cathodes were prepared by pressing a blend of 90 weight percent (w/o)  $\text{MnO}_2$ , 5 w/o acetylene black, and 5 w/o Teflon organic binder onto a stainless steel screen (SUS304, Dainippon Screen Company, Limited). The prepared cathodes were dried under vacuum at  $150^\circ\text{C}$  for more than 12h before use. The anodes were prepared by pressing a lithium sheet onto a stainless steel screen reinforced with 1 mm-thick nickel plate ( $15 \times 20 \text{ mm}^2$ ).

A lithium sheet was made by pressing a tip which was cut from a rod (99.9% purity, Rare Metallic Company, Limited). A cathode and anode separated by nonwoven cloth were placed in a cavity of a container and ca. 0.2 ml of electrolyte was introduced. A container consisted of two insulated stainless steel plates (5 mm-thick) separated by a 2 mm-thick Teflon spacer in which a  $25 \times 35 \text{ mm}^2$  window was made. After the electrodes and separator were placed in the cavity, the cell was mechanically sealed. Internal electrode contact was attained by means of a stainless steel spring. The electrolyte used was 1M  $\text{LiClO}_4$ -propylene carbonate—(PC)/tetrahydrofuran(THF) (1:1) solution. All procedures were carried out in a dry box. Other sets of experimental conditions are given in the Results section.

## Results

**Continuous discharge curve.**—Figure 1 shows the continuous discharge curves of HEMD(250) and HEMD(400) in 1M  $\text{LiClO}_4$  PC/THF solution. Each curve represents the average for more than 20 cells. The cells were discharged at  $0.1 \text{ mA cm}^{-2}$  ( $3.5 \text{ mA g}^{-1}$  of  $\text{MnO}_2$ ) at  $30^\circ\text{C}$ . The cut-off voltage was 1.5V.

The analytical values of the samples, Mn w/o,  $\text{MnO}_2$  w/o, and  $x$  in  $\text{MnO}_x$ , were 62.27, 95.39 and 1.968 for HEMD(250), and 62.62, 96.56, and 1.975 for HEMD(400), respectively. As can be seen in Fig. 1, the working voltage of HEMD(250) was ca. 130 mV higher than that of HEMD(400) at the initial stage of the reduction. Both samples exhibited a flat portion in the discharge curve at 2.98V and 2.84V for HEMD(250) and HEMD(400), respectively. The shape of the discharge curve of HEMD(400) was more flat than that of HEMD(250), as was already reported (1-6, 8). The discharge capacities were 230-250 and 240-270  $\text{mAh g}^{-1}$  based on the sample weight for HEMD(250) and HEMD(400), respectively, if all data examined were included. Utilization for both samples was calculated to be 80-90% based on the available  $\text{Mn}^{4+}$  ions in a solid matrix in this experimental condition.

**Open-circuit voltage curves.**—In order to measure the open-circuit voltage curves during the electrochemical reduction of HEMD, intermittent discharge tests, 3h on and 5h off, were carried out at  $0.1 \text{ mA cm}^{-2}$  ( $3.5 \text{ mA g}^{-1}$  of  $\text{MnO}_2$ ). The cell voltages at 5h after the current was switched off were plotted in Fig. 2 as a function of reduc-

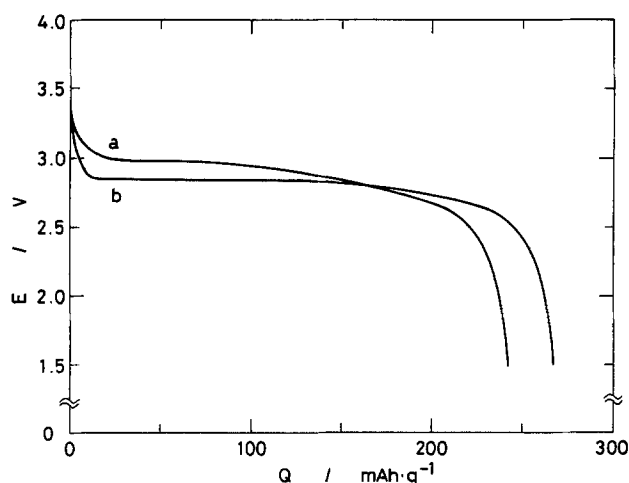


Fig. 1. Continuous discharge curves of EMDs heat-treated at (a)  $250^\circ\text{C}$  and (b)  $400^\circ\text{C}$ , for 7 days. Electrolyte: 1M  $\text{LiClO}_4$  PC/THF (1:1). Current:  $0.1 \text{ mA cm}^{-2}$  ( $3.5 \text{ mA g}^{-1}$ ).

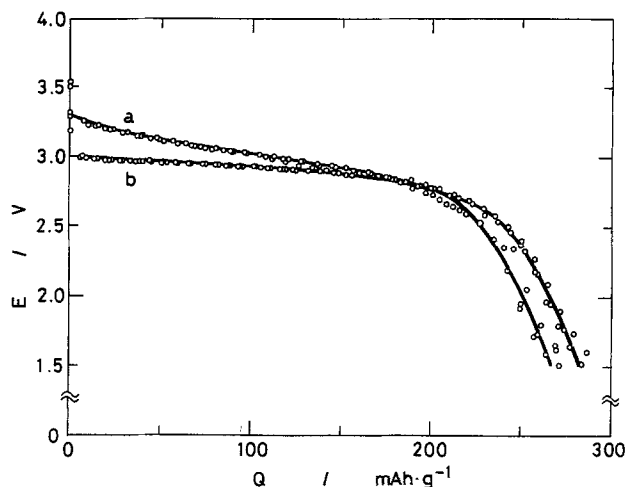


Fig. 2. Open-circuit voltage curves of EMDs heat-treated at (a)  $250^\circ\text{C}$  and (b)  $400^\circ\text{C}$ , for 7 days. Electrolyte: 1M  $\text{LiClO}_4$  PC/THF (1:1).

tion degree of  $\text{mAh g}^{-1}$  based on the sample weight used. Both curves in Fig. 2 contain the results for 3 cells. A different mode of intermittent discharge tests, 6h on and 18h off, was also examined. The observed open-circuit voltages, however, were within the scatter of the results shown in Fig. 2. Initial open-circuit voltages were 3.5-3.6V for both HEMDs. HEMD(250) shows higher open-circuit voltages in 0-190  $\text{mAh g}^{-1}$  of reduction degree than that of HEMD(400). Although the voltage plateaus for both samples were observed in a low-rate discharge curve, any voltage plateaus were not observed in the open-circuit voltage curves. Open-circuit voltages of HEMD(250) decreased continuously from 3.3V to 1.5V as a function of reduction degree. The open-circuit voltages of HEMD(400) were seemingly more flat than that of HEMD(250). They, however, decreased almost linearly from 3.0V to 2.9V as a function of reduction degree. Utilization was calculated to be 90-95% based on the available  $\text{Mn}^{4+}$  ions in a solid matrix for both HEMDs. Utilization of HEMD(400) was slightly greater than that of HEMD(250), as was shown in Fig. 1 and 2.

**XRD pattern change during the reduction of HEMD.**—Figures 3 and 4 show the x-ray diffractational pattern changes with progressive reduction of HEMD(250) and HEMD(400), respectively. Since the locations of diffraction lines ( $2\theta$ ), and the shapes of lines as a function of reduction degree, were important in considering the structure changes during the reduction of HEMDs, the observed XRD patterns at the different depths of discharge were given in the same figure.

The HEMD(250) sample shows 4 main diffraction lines at 3.83, 2.42, 2.12, and  $1.63 \text{ \AA}$  in  $d$ -values, which are denoted as peaks (a), (b), (c), and (d) in Fig. 3. Some additional diffraction lines were also observed in XRD data. These peaks, however, were not well-defined, due to the distortion in shapes and the weakness in their intensities. Peak (a) in Fig. 3 seems to be shifted continuously toward the lower diffraction angle from  $29.3^\circ$  to  $25.0^\circ$  in  $2\theta$ , which corresponds to the expansion from  $3.83 \text{ \AA}$  to  $4.47 \text{ \AA}$  in  $d$ -values with progressive reduction of HEMD(250). Peak (b) also seems to be shifted slightly, from  $47.2^\circ$  to  $46.2^\circ$  in  $2\theta$ . Peaks (c) and (d), however, did not shift continuously. The diffraction intensities of peaks (c) and (d) were slightly decreased as the reduction proceeded and new diffraction lines appeared at the neighboring positions. At 100  $\text{mAh g}^{-1}$  or 125  $\text{mAh g}^{-1}$  of reduction degree, these peaks coexisted clearly in XRD data and the diffraction line at ca.  $86.5^\circ$  in  $2\theta$  became apparent in its shape. Further reduction of the sample resulted in the disappearance of peaks (c) and (d) and the appearance of new peaks substituting for peaks (c) and (d). From 100  $\text{mAh g}^{-1}$  to 245  $\text{mAh g}^{-1}$  of reduction degree, the new peaks continuously shifted toward lower diffraction angles, indicating continuous lattice expansion during the latter part of HEMD(250) reduction. As can be seen in Fig. 3, reducing HEMD(250) in a

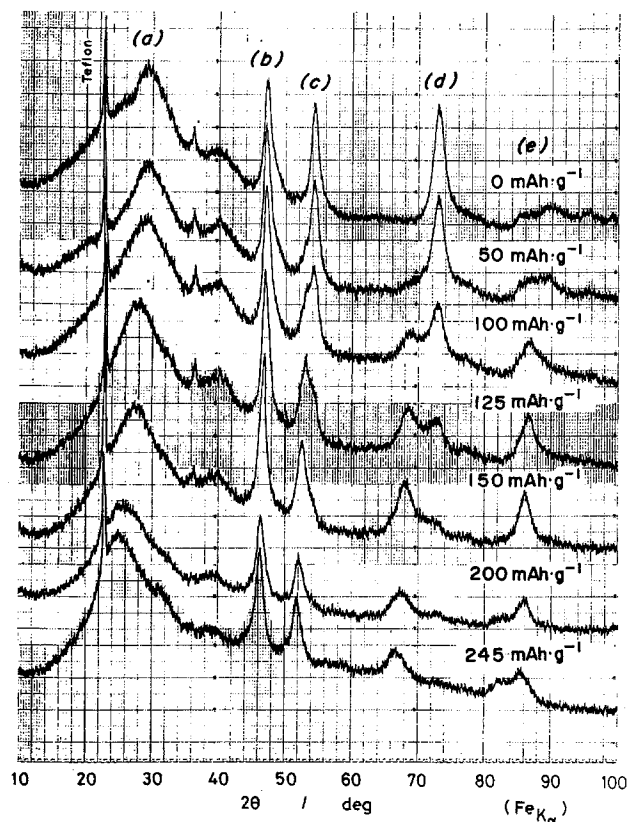


Fig. 3. X-ray diffractograms of heat-treated EMD (250°C, 7 days) during the reduction in a lithium nonaqueous cell.

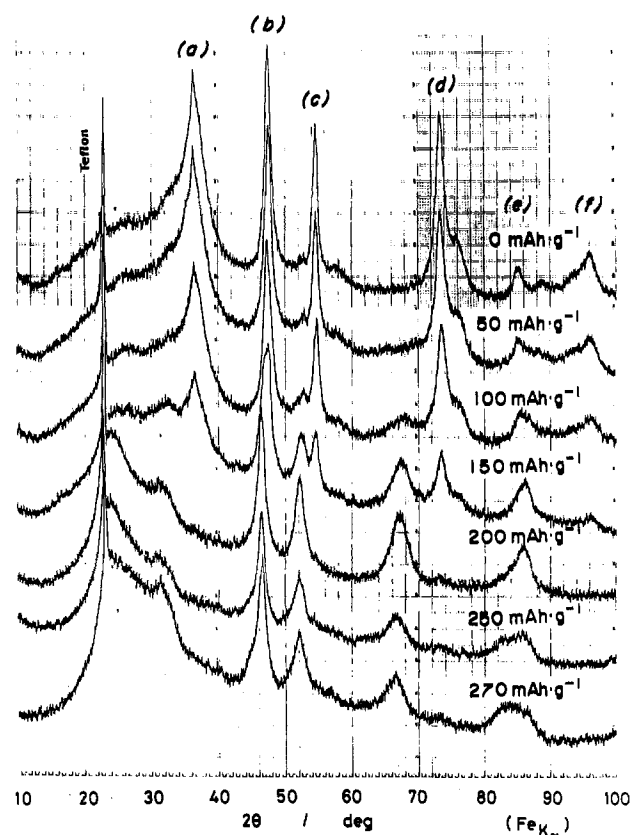


Fig. 4. X-ray diffractograms of heat-treated EMD (400°C, 7 days) during the reduction in a lithium nonaqueous cell.

lithium nonaqueous cell does not give a line-richer pattern. A selective broadening at peak (a) still exists in XRD patterns of all reduced HEMD(250) samples. The series of XRD patterns in Fig. 3 indicates that there are no destruc-

tive changes in structure during the electrochemical reduction of HEMD(250) in lithium nonaqueous cells.

Figure 4 shows the XRD pattern changes of HEMD(400) during the reduction. The diffraction pattern of HEMD(400) is very similar to that of pyrolusite ( $\beta\text{-MnO}_2$ ). The peaks (a)-(e) may be indexed as (110), (101), (111), (211), (002), and (301), respectively, assuming a tetragonal lattice. Of these, diffraction lines at 2.42, 2.12, and 1.63 Å in  $d$ -values were almost the same as those observed in HEMD(250). In reducing the sample, the peaks (a), (c), (d), and (f) became weakened in their intensities, and new peaks substituting for the peaks (a), (c), and (d) became clear in their line shapes. At 100  $\text{mAh}\cdot\text{g}^{-1}$  or 150  $\text{mAh}\cdot\text{g}^{-1}$  of reduction degree, the coexistence of peaks (c) and (d) and their relatives was evidently observed in XRD patterns. For further reductions, these peaks continuously shifted their positions toward lower diffraction angles. The peaks (b) and (e) seem to be continuously shifted slightly in their positions. However, if the line shapes of these peaks were carefully observed, especially the peak (b), one can recognize that the apparent peak shifts are due to the changes in intensities of the overlapping two diffraction lines, which are very closely situated.

General observations in XRD data of HEMD(400) are the same as those of HEMD(250), *i.e.*, no destructive changes are seen in structure during the electrochemical reduction of HEMD(400) in lithium nonaqueous cells.

**Heating the reduction product of HEMDs.**—In order to confirm the existence of lithium ions in a solid matrix, the samples having several reduction degrees were heated at 700°C for 3h in air. Before heating, the electrochemically reduced samples were rinsed thoroughly with THF. The product of the HEMD sample, which was soaked in an electrolyte and then heated at 700°C, was bixbyite ( $\alpha\text{-Mn}_2\text{O}_3$ ). The reduced samples below *ca.* 130  $\text{mAh}\cdot\text{g}^{-1}$  of reduction degrees for both HEMDs gave the mixed products of bixbyite and cubic spinel. The deeply reduced samples above *ca.* 170  $\text{mAh}\cdot\text{g}^{-1}$  gave a cubic spinel which has an identical XRD pattern to  $\text{LiMn}_2\text{O}_4$  (cubic:  $a = 8.24\text{Å}$ ). Figure 5 shows the XRD pattern of the reduction product of HEMD(250) at 245  $\text{mAh}\cdot\text{g}^{-1}$  of reduction degree and its product heated at 700°C for 3h. Miller indexes in Fig. 5 were given based on a cubic lattice ( $a = 8.24\text{Å}$ ). The final reduction product of HEMD(400) also gave the same product.

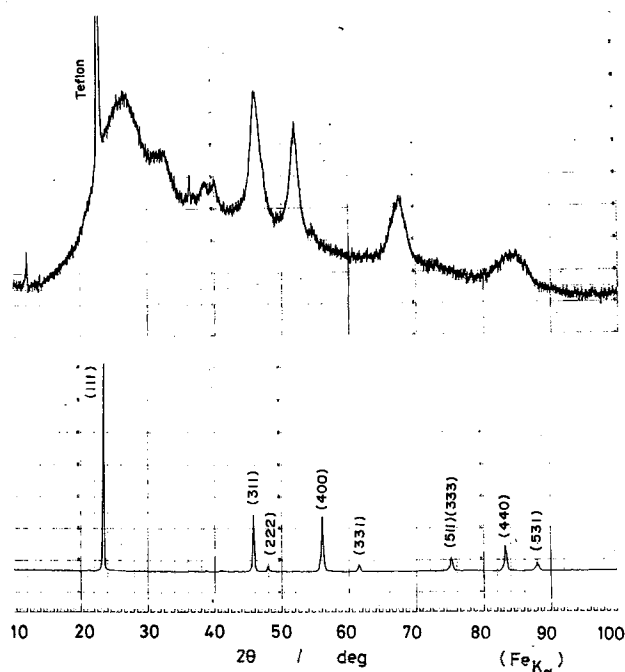


Fig. 5. X-ray diffractograms of a reduction product of heat-treated EMD (250°C, 7 days) and its heated product at 700°C for 3h in air.

These results combined with the results on the XRD pattern changes during the electrochemical reduction of HEMDs in lithium nonaqueous cell indicate that the reaction consists of electron injection and lithium ion insertion into a solid matrix without the destruction of the core EMD structure.

### Discussion

**Structural changes during the reduction.**—The specific description of the crystal structure of HEMD together with EMD is necessary to discuss the reaction mechanisms of HEMD in lithium nonaqueous cells. In previous papers (7-9), we have discussed the crystal structures of EMD and HEMD in relation to the electrochemical reactivities and physicochemical properties. Although there are several arguments on the crystal structure of EMD, there is general agreement that EMD has at least pyrolusite ( $1 \times 1$ ) and ramsdellite ( $1 \times 2$ ) domains in a hexagonally close-packed oxygen matrix. According to our previous results (8, 9), EMD does not change its core structure on heating. The difference between EMD and HEMD is the concentration and distribution of ramsdellite ( $1 \times 2$ ) and pyrolusite ( $1 \times 1$ ) (possibly epsilon-MnO<sub>2</sub>) domains in a solid matrix (7, 9, 10). Since the unit cell volume of ramsdellite is two times greater than that of pyrolusite, some main diffraction lines from the intergrowth products of pyrolusite and ramsdellite may be described assuming the tetragonal sublattice. For example, if we assume the Miller indexes of the main peaks (b), (c), and (d) in Fig. 3 for HEMD(250) to be (101), (111), and (211), the lattice constants of a tetragonal sublattice are calculated to be  $a = 4.40\text{\AA}$  and  $c = 2.90\text{\AA}$ . Similarly, the lattice constants of HEMD(400) are calculated to be  $a = 4.39\text{\AA}$  and  $c = 2.86\text{\AA}$  by assuming the Miller indexes of the main peaks (a)-(e) in Fig. 4 to be (110), (101), (111), (211), (002), and (301). Thus, HEMD(250) and HEMD(400) have the same tetragonal sublattice constants.

Since no destructive changes in structure have been observed in Fig. 3 and 4 for HEMD(250) and HEMD(400), respectively, the structural changes of HEMD due to the electrochemical reduction may be described using an assumed tetragonal sublattice. In order to obtain tetragonal sublattice constants in reduced forms of HEMDs as a function of reduction degree, the corresponding main peaks (b), (c), (d), and (e) in Fig. 3 and 4 are assumed to be (101), (111), (211), and (002). Figure 6 shows the thus-obtained lattice constants from XRD data in Fig. 3 and 4. Open triangles and circles in Fig. 6 indicate the changes in dimension of a lattice during the electrochemical reduction of HEMD(250) and HEMD(400), respectively, in lithium nonaqueous cell. As can be seen in Fig. 6, HEMD(250) and HEMD(400) behave similarly in the lattice constants vs. the

reduction degree plots. During the first ca. 50% of reduction (0-150 mAh g<sup>-1</sup>), a tetragonal sublattice having  $a = 4.39\text{-}4.40\text{\AA}$  and  $c = 2.86\text{-}2.90\text{\AA}$  does not change in its lattice constant. At ca. 30-50% of reduction, lattice expansion in the  $a$ -axis and a little shrinkage in the  $c$ -axis become apparent, together with the coexistence of two phases having different lattice constants. In 30-90% reduction, the  $a$ -axis of a new tetragonal sublattice expands continuously with progressive reduction, while noticeable change in the  $c$ -axis was not observed.

In comparing a new tetragonal sublattice of HEMD(400) with that of HEMD(250), the lattice constant of the former  $a$ -axis is greater than that of the latter  $a$ -axis in the 30-60% reduction. However, the deeply reduced HEMD(250) and HEMD(400) samples exhibited almost the same lattice constant, i.e.,  $a = \text{ca. } 5\text{\AA}$  and  $c = \text{ca. } 2.85\text{\AA}$ , suggesting that HEMD(250) and HEMD(400) formed almost the same crystal structure as a final reduction product.

Such a tetragonal (sub)lattice having lithium ions in a matrix reminds us of the reduction product of RuO<sub>2</sub> in a lithium nonaqueous cell (11, 12). In reducing RuO<sub>2</sub> having the rutile structure, lithium ions are inserted into octahedral sites with changes in its lattice constant and oxygen parameter (12). The electrochemical reduction of RuO<sub>2</sub> proceeds topotactically in two phases. The reduction product of RuO<sub>2</sub> has primarily a tetragonal lattice ( $a = 4.980\text{\AA}$ ,  $c = 2.774\text{\AA}$ ) with oxygen parameter 0.26 (space group P4<sub>2</sub>/mnm) (12), more closely related to the NiAs-type structure, i.e., a hexagonally close-packed arrangement of oxygen ions in which half of the octahedral sites are occupied by Ru<sup>3+</sup> ions and half of the octahedral sites by Li<sup>+</sup> ions (11). In the Li<sub>x</sub>RuO<sub>2</sub> system, the alternation of space groups from the rutile type to the NiAs-type, together with lattice expansion, induce a two-phase electrochemical reaction in a topotactic manner (12).

Nardi (6) suggested a structural change in the MnO<sub>2</sub> from its initial hexagonal close-packed configuration to a cubic close-packed configuration in the 10-40% reduction of MnO<sub>2</sub> from his electrochemical study on non-heat-treated EMD and heat-treated EMD (350°C, 8h). Although the results described here well agree with his observations, the alternation from a hexagonally close-packed O<sup>2-</sup> arrangement to a cubic close-packed structure is hardly recognized in our XRD study. Burns (10) also suggested the formation of a Li<sub>x</sub>Mn<sub>2</sub>O<sub>4</sub> phase having a spinel framework with tetragonal symmetry as the deep discharge product of EMD in lithium nonaqueous cells. A tetragonal Li<sub>x</sub>Mn<sub>2</sub>O<sub>4</sub> phase ( $a = 5.63\text{\AA}$ ,  $c = 9.16\text{\AA}$ ) (8, 13, 14) having a spinel framework (space group; I4<sub>1</sub>/amd), however, was not observed in this experimental condition even for over-discharged HEMD samples.

Figure 7 shows an idealized crystal structure of LiMnO<sub>2</sub>, having a tetragonal lattice (space group P4<sub>2</sub>/mnm; oxygen parameter 0.25) and its calculated XRD patterns with  $a = 5.0\text{\AA}$  and  $c = 2.85\text{\AA}$ . The observed 4 main peaks from the reduction product of HEMDs were explained as (200)(101), (210)(211), (220)(211), and (301)(002). The observed intensity of the (110) line and the broad diffraction line at ca. 4.4-4.6Å in  $d$ -value were not explained by a simple structural model in Fig. 7. The location of a broad diffraction line at ca. 4.4-4.6Å, however, may be explained as a (110) line from an orthorhombic unit cell which consists of two tetragonal sublattices, i.e.,  $a = \text{ca. } 2 \times b\text{\AA}$ ,  $b = 4.9\text{-}5.0\text{\AA}$ , and  $c = 2.82\text{-}2.86\text{\AA}$ . Assuming an orthorhombic unit cell having  $a = 10.27\text{\AA}$ ,  $b = 4.93\text{\AA}$ , and  $c = 2.85\text{\AA}$ , indexes (h, k, l) for all the diffraction lines observed from the reduction product of HEMDs at ca. 250 mAh g<sup>-1</sup> of reduction degree may be assigned as shown in Table I, together with the assignment assuming a tetragonal unit cell.

As can be seen in Table I, the reduction products obtained from HEMD(250) and HEMD(400) have the same  $d$ -values of the diffraction lines, indicating that both products contained the same crystal structure. A possible structure having an orthorhombic unit cell with  $a = \text{ca. } 10\text{\AA}$ ,  $b = \text{ca. } 5\text{\AA}$ , and  $c = \text{ca. } 2.85\text{\AA}$ , may be ramsdellite-type structure [(1 × 2)-tunnel structure] or (1 × 3)-tunnel structure having a hexagonally close-packed arrangement of oxygen in which lithium ions are located at octahedral sites.

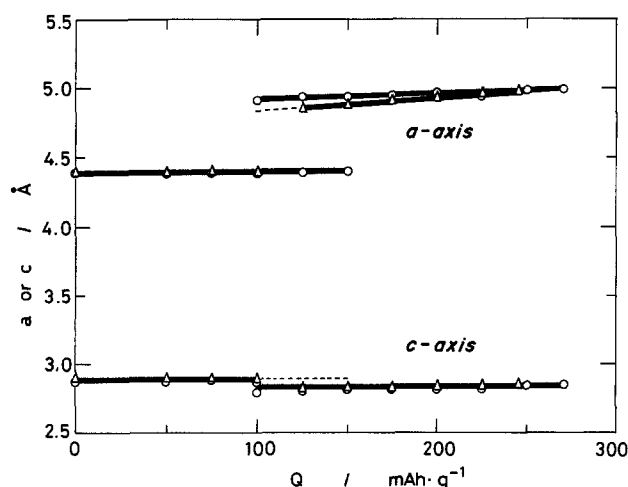


Fig. 6. The lattice parameter vs. the reduction degree plots for the electrochemical reduction of HEMDs in lithium nonaqueous cell. Lattice parameters were obtained assuming the peaks (b), (c), (d), and (e) in Fig. 3 and 4 to be (101), (111), (211), and (002) in a tetragonal sublattice. Open circles and triangles indicate the results from HEMD(400) and HEMD(250), respectively.

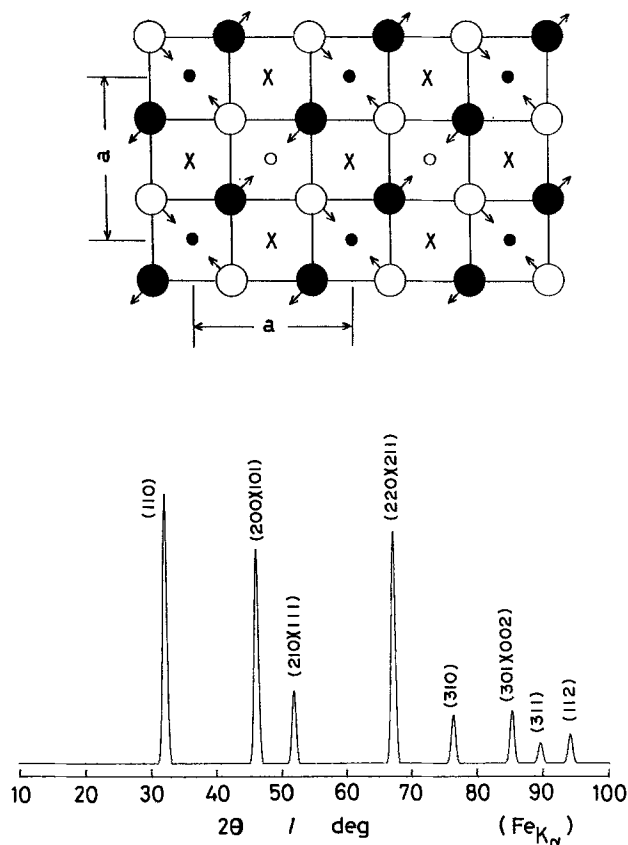


Fig. 7. An idealized crystal structure of  $\text{LiMnO}_2$  having a tetragonal lattice (space group  $P4_2/mnm$ ; oxygen parameter 0.25) (top), and its calculated XRD patterns (bottom), with  $a = 5.0\text{Å}$  and  $c = 2.85\text{Å}$ . Arrows indicate the possible Jahn-Teller distortion of the  $[\text{Mn}^{3+}\text{O}_6]^{2-}$  unit octahedron. Xs indicate the octahedral sites in which lithium ions are located.

**Reduction mechanism of HEMD in lithium nonaqueous cells.**—Since the structural changes from HEMD(250) and HEMD(400) to a new  $\text{Li}_x\text{MnO}_2$  phase can be described as lattice parameter changes using a tetragonal sublattice, we can discuss the reduction mechanism of HEMD in lithium nonaqueous cell.

During the first half of the reduction, an HEMD phase having a tetragonal sublattice ( $a = 4.39\text{--}4.40\text{Å}$ ,  $c = 2.85\text{--}2.90\text{Å}$ ) is progressively converted into a new  $\text{Li}_x\text{MnO}_2$  phase having an expanded tetragonal sublattice ( $a = 4.9\text{--}5.0\text{Å}$ ,  $c = 2.82\text{--}2.85\text{Å}$ ), and this is a two-phase reaction. During this period, lithium ions are inserted into octahedral sites in an HEMD matrix by changing its sublattice parameters with the aids of thermal vibration and

electric field across a phase boundary. Since the phase boundary between HEMD phase and a new  $\text{Li}_x\text{MnO}_2$  phase moves with progressive discharge, an internal stress in a newly formed  $\text{Li}_x\text{MnO}_2$  phase may induce a lattice disorder in the matrix. Consequently, such a progressive phase alternation was not observed by XRD method in the first ca. 25% reduction, until an internal stress was removed and a well-ordered  $\text{Li}_x\text{MnO}_2$  phase was increased.

In the 30-90% reduction, lithium ions are inserted into unoccupied octahedral sites and migrate through octahedral sites, possibly via tetrahedral sites due to energetic preference (10), in a new  $\text{Li}_x\text{MnO}_2$  phase. Further lithium ion concentration and  $\text{Mn}^{3+}$  formation result in a continuous expansion of tetragonal sublattice in a  $\text{Li}_x\text{MnO}_2$  phase ( $x = \text{ca. } 0.3\text{--}0.9$ ). This is a homogeneous phase reaction. A tetragonal sublattice in a new  $\text{Li}_x\text{MnO}_2$  may be related to the NiAs-type structure as was discussed in the previous section. As far as the NiAs-type structure is concerned, epsilon- $\text{MnO}_2$  has been described as having the NiAs-type structure (15), which is also a particular end member of gamma- $\text{MnO}_2$  (9, 15).

Since the electrochemical reaction of HEMD proceeds in two phases in the first half of the reduction, the reversible electrode potential is expected to be a constant as a function of reduction degree. The reversibility, however, is poor in this region (16). In this two-phase region, HEMD phase and a formed  $\text{Li}_x\text{MnO}_2$  phase coexist in a matrix. HEMD still contains a structural water, more properly  $\text{OH}^-$  ions in a matrix, because of the structural and physicochemical nature of  $\text{MnO}_2$  (17). If an external current is switched off in this two-phase region, HEMD-contained  $\text{OH}^-$  ions in a matrix may be equilibrated with  $\text{H}_2\text{O}$ , which is a contamination on particles or in the electrolyte used (normally below  $100\text{ mg l}^{-1}$ ), and a  $\text{Li}_x\text{MnO}_2$  phase may be also equilibrated with  $\text{Li}^+$  ions in the electrolyte, together with an equilibrium between HEMD phase and a new  $\text{Li}_x\text{MnO}_2$  phase. Since such (two or three) reactions take place during an open-circuit condition, observed open-circuit voltages in Fig. 2 and that of long-term tests on the OCV recovery (6) may show a mixed potential between them. Characteristic features of a two-phase reaction may be reflected in the shapes of the low-rate discharge curve, i.e., there is a flat portion in the discharge curve.

In the latter half of the reduction, the reaction proceeds in a homogeneous phase. Although the rechargeability of HEMD is described as poor even at a limited depth of discharge (5), a new  $\text{Li}_x\text{MnO}_2$  phase is highly rechargeable in a lithium nonaqueous cell, i.e., typically  $\text{Li}_x\text{MnO}_2$  ( $x = \text{ca. } 0.3\text{--}0.9$ ), which corresponds to ca.  $150\text{--}200\text{ mAh g}^{-1}$  of rechargeable capacity (16). Reversible electrode potentials in this homogeneous region and a more specific description of the crystal structure of this new  $\text{Li}_x\text{MnO}_2$  phase will be discussed in a separate paper in relation to the rechargeability of HEMD in a lithium nonaqueous cell.

### Summary

In this paper, we have dealt with the reduction mechanism of heat-treated EMD in lithium nonaqueous cells. A series of XRD examinations indicated that the reaction consisted of electron injection and lithium ion insertion into a solid matrix without the destruction of the core structure of EMD. The structural changes during the electrochemical reduction of HEMD were described assuming a tetragonal sublattice.

During the first half of the reduction, an HEMD phase having a tetragonal sublattice ( $a = 4.39\text{--}4.40\text{Å}$ ,  $c = 2.86\text{--}2.90\text{Å}$ ) was converted into a new  $\text{Li}_x\text{MnO}_2$  phase having an expanded tetragonal sublattice ( $a = 4.9\text{--}5.0\text{Å}$ ,  $c = 2.82\text{--}2.86\text{Å}$ ), i.e., a two-phase reaction. In the 30-90% reduction, lithium ions are inserted into unoccupied octahedral sites and migrate in a new  $\text{Li}_x\text{MnO}_2$  phase, which is characterized by a continuous increase in  $a$ -axis based on a tetragonal sublattice as a function of reduction degree, i.e., a homogeneous phase reaction. The possible crystal structure of the deep discharge product  $\text{Li}_x\text{MnO}_2$  ( $x > 0.8$ ) was discussed assuming a tetragonal unit cell ( $a = \text{ca. } 5\text{Å}$ ,  $c = \text{ca. } 2.85\text{Å}$ ) having the NiAs-type structure by analogy with  $\text{Li}_x\text{RuO}_2$  and an orthorhombic unit cell, i.e.,  $a = 2 \times b\text{Å}$ ,

Table I. Analysis of x-ray diffraction data on the deep discharge product of heat-treated electrolytic  $\text{MnO}_2$  in lithium nonaqueous cell

Peak No.	$d_{\text{obs}}/\text{Å}^a$	$d_{\text{obs}}/\text{Å}^b$	(h,k,l) <sup>c</sup>	$d_{\text{calc}}/\text{Å}^c$	(h,k,l) <sup>d</sup>	$d_{\text{calc}}/\text{Å}^d$
1	4.47	4.4-4.6	—	—	(1,1,0)	4.44
2	3.5-3.6	3.60	(1,1,0)	3.52	(2,1,0)	3.56
3	2.47	2.45	(2,0,0)	2.49	(2,0,1)	2.49
			(1,0,1)	2.48		
4	2.22	2.20	(2,1,0)	2.23	(2,1,1)	2.23
			(1,1,1)	2.22		
5	1.76	1.76	(2,2,0)	1.76	(4,1,1)	1.78
			(2,1,1)	1.76		
6	1.47	1.48	—	—	(601)	1.47
7	1.43	1.43	(0,0,2)	1.43	(0,0,2)	1.43
			(3,0,1)	1.44		

<sup>a</sup> Reduction product of HEMD(250) at  $245\text{ mAh g}^{-1}$  of reduction degree.

<sup>b</sup> Reduction product of HEMD(400) at  $250\text{ mAh g}^{-1}$  or reduction degree.

<sup>c</sup> Assuming tetragonal unit cell ( $a = 4.98\text{Å}$ ,  $c = 2.86\text{Å}$ ).

<sup>d</sup> Assuming orthorhombic unit cell ( $a = 10.27\text{Å}$ ,  $b = 4.93\text{Å}$ ,  $c = 2.85\text{Å}$ ).

$b = ca. 5\text{\AA}$ ,  $c = ca. 2.85\text{\AA}$ . From these, assuming an orthorhombic unit cell having  $a = 10.27\text{\AA}$ ,  $b = 4.93\text{\AA}$ , and  $c = 2.85\text{\AA}$ , all diffraction lines from the reduction products of HEMD can be indexed.

### Acknowledgments

The authors wish to thank Professor R. Burns of MIT for his helpful discussion on the crystal structure of a reduced form of HEMD. The present work was partially supported by grants in aid for Scientific Research from the Ministry of Education, Science, and Culture, of Japan, and Asahi Glass Kogyo Gijutsu Shoreikai.

Manuscript submitted Nov. 23, 1988; revised manuscript received March 29, 1989.

Osaka City University assisted in meeting the publication costs of this article.

### REFERENCES

1. H. Ikeda, T. Saito, and H. Tamura, in "Manganese Dioxide Symposium," **1**, 384 (1975).
2. H. Ikeda, M. Hara, S. Narukawa, and S. Nakaido, *ibid.*, **2**, 395 (1980).
3. H. Ikeda, S. Narukawa, and S. Suenaga, *ibid.*, 414.
4. H. Ikeda and S. Narukawa, *J. Power Sources*, **9**, 329 (1983).
5. G. Pistoia, *This Journal*, **129**, 1861 (1982).
6. J. C. Nardi, *ibid.*, **132**, 1787 (1985).
7. T. Ohzuku, H. Higashimura, and T. Hirai, *Electrochim. Acta*, **29**, 779 (1984).
8. T. Ohzuku, Y. Kogo, and T. Hirai, in "Manganese Dioxide Symposium," **3**, 391 (1985).
9. T. Ohzuku and T. Hirai, *Progress in Batteries & Solar Cells*, **7**, 31 (1988).
10. R. G. Burns, in "Manganese Dioxide Symposium," **3**, 519 (1985).
11. I. J. Davidson and J. E. Greedan, *J. Solid State Chem.*, **51**, 104 (1984).
12. T. Ohzuku, T. Kunishi, and T. Hirai, In preparation.
13. M. M. Thackeray, W. I. F. David, P. G. Bruce, and J. B. Goodenough, *Mater. Res. Bull.*, **18**, 461 (1983).
14. T. Ohzuku, M. Kitagawa, and T. Hirai, in "Abstracts of the 29th Battery Symposium in Japan," p. 135, Ube, Oct. 1988.
15. R. Giovanoli, "Manganese Dioxide Symposium," **2**, 113 (1980).
16. T. Ohzuku, K. Sawai, and T. Hirai, in "Abstracts of the 29th Battery Symposium in Japan," p. 137.
17. P. Ruetschi, *This Journal*, **131**, 2737 (1984).

## Compatibility of Molybdenum Current Collectors in Lithium-Alloy/Iron Disulfide Cell Environment

Ram A. Sharma

General Motors Research Laboratories, Department of Physical Chemistry, Warren, Michigan 48090-9055

### ABSTRACT

Stability of molybdenum metal was determined in a Li-Al or Li-Si/FeS<sub>2</sub> cell environment using a steady-state potential technique and a cyclic voltammetry technique. By the steady-state potential technique, molybdenum was found chemically stable with lithium chloride-potassium chloride eutectic electrolyte at potentials smaller than  $\sim 1.5\text{V}$  with respect to a lithium-aluminum reference electrode at about 700 K. It reacted with the electrolyte at the potentials equal to or greater than  $\sim 1.5\text{V}$ . However, this reaction was probably caused by some impurities such as titanium or zirconium in the molybdenum. Addition of lithium sulfide to the electrolyte suppressed the above reaction, but a molybdenum sulfide forming reaction started at  $\sim 1.55\text{V}$  with respect to the Li-Al reference electrode. The reaction of molybdenum with the electrolyte forming a chloride occurred at about 2.1V. These observations were in agreement with those made by the cyclic voltammetry technique. Continuous sweeping from 1 to 1.85V indicated that molybdenum was not passivated by sulfidation at 700 K in these melts. However, the sulfidation reaction may not be too severe to preclude the use of molybdenum metal structures as current collectors in FeS<sub>2</sub> electrodes.

In studies of lithium-aluminum or lithium-silicon/iron disulfide compact cells, high self-discharge is observed with increasing test duration. In these cells, a molybdenum metal structure as current collector in the iron disulfide electrode, and boron nitride cloth separator to electronically isolate the positive and negative electrodes in LiCl-KCl eutectic electrolyte, are used. The cell is operated at  $\sim 700\text{K}$  and undergoes two major voltage plateaus at 1.34 and 1.75V corresponding to two compounds, FeS and FeS<sub>2</sub>, respectively, during cycling (1). The molybdenum current collector has to be chemically stable with LiCl-KCl electrolyte saturated with Li<sub>2</sub>S at the beginning and during most of charging, and with the practically pure electrolyte near the end of charging under these cell operating conditions. Post-mortem studies of these cells indicated a slight molybdenum current collector reaction with sulfur species in the positive electrode forming molybdenum sulfide. The boron nitride separator was also observed to develop electronic conduction.

A static immersion test indicated practically no reaction of molybdenum metal with the electrolyte saturated with Li<sub>2</sub>S during a 1000h test at 725 K; only a purple coloration of the sample was observed. Studies at Argonne National Laboratory have also shown molybdenum to be corrosion resistant in the above melts (2). Raleigh *et al.* (3) have also reported molybdenum to be stable in these melts, but the stability has been reported to be due to passivation.

This investigation was conducted to determine the stability of molybdenum in an environment similar to that of a Li-alloy/LiCl-KCl eutectic/iron disulfide cell and at typical charge/discharge potentials.

### Experimental

*Steady-state potential technique.*—All of the experimental work was done in a helium atmosphere glove box. The data were obtained by a cell (Fig. 1) in which a molybdenum electrode, a stainless steel screen electrode, and lithium chloride-potassium chloride electrolyte were used. The two electrodes sandwiched the boron nitride separator when it was used and their potentials were set by two separate electrical circuits and a lithium-silicon reservoir counterelectrode in the cell. The electrical circuit shown in Fig. 2 and described in Ref. (4) consisted of a dc power supply, a dual channel recorder for recording potential and current, and a digital meter to measure the potential and the current. A tubular furnace (150 mm high, 75 mm diam) was used in conjunction with a variable transformer to heat the cell. Chromel-Alumel thermocouples and a millivolt potentiometer were used for temperature measurements.

*Electrodes.*—Various types of molybdenum electrodes were used. They were made from a molybdenum sheet or bar of 99.95% purity. The bar and sheet were manufactured from molybdenum powder of the composition given in Table I.